

Article

Effects of the Solvent Vapor Exposure on the Optical Properties and Photocatalytic Behavior of Cellulose Acetate/Perylene Free-Standing Films

Gustavo Coderch ¹, Alexander Cordoba ¹, Oscar Ramírez ^{1,2,3}, Sebastian Bonarrrd ^{2,3}, Angel Leiva ¹, Marleen Häring ⁴, David Díaz Díaz ^{2,3,4,*} and Cesar Saldias ^{1,*}

¹ Departamento de Química Física, Facultad de Química y de Farmacia, Pontificia Universidad Católica de Chile, Macul, Santiago 7820436, Chile; gustavo.coderch@uc.cl (G.C.); acordoba@uc.cl (A.C.); ogramirez@uc.cl (O.R.); aleivac@uc.cl (A.L.)

² Instituto Universitario de Bio-Organica Antonio Gonzalez, Universidad de La Laguna, Avda. Astrofísico Francisco Sanchez, 38206 La Laguna, Spain; sbonarrrd@ull.edu.es

³ Departamento de Química Orgánica, Universidad de La Laguna, Avda. Astrofísico Francisco Sánchez, S/N, 38206 La Laguna, Spain

⁴ Institut für Organische Chemie, Universität Regensburg, Universitätsstr. 31, 93053 Regensburg, Germany; marleen.haering@chemie.uni-regensburg.de

* Correspondence: ddiazdiaz@ull.edu.es (D.D.D.); casaldia@uc.cl (C.S.)

Abstract: The search to deliver added value to industrialized biobased materials, such as cellulose derivatives, is a relevant aspect in the scientific, technological and innovation fields at present. To address these aspects, films of cellulose acetate (CA) and a perylene derivative (Pr) were fabricated using a solution-casting method with two different compositions. Consequently, these samples were exposed to dimethylformamide (DMF) solvent vapors so that its influence on the optical, wettability, and topographical properties of the films could be examined. The results demonstrated that solvent vapor could induce the apparent total or partial preferential orientation/migration of Pr toward the polymer–air interface. In addition, photocatalytic activities of the non-exposed and DMF vapor-exposed films against the degradation of methylene blue (MB) in an aqueous medium using light-emitting diode visible light irradiation were comparatively investigated. Apparently, the observed improvement in the performance of these materials in the MB photodegradation process is closely linked to the treatment with solvent vapor. Results from this study have allowed us to propose the fabrication and use of the improved photoactivity “all-organic” materials for potential applications in dye photodegradation in aqueous media.

Keywords: films; biobased materials; photodegradation



Citation: Coderch, G.; Cordoba, A.; Ramírez, O.; Bonarrrd, S.; Leiva, A.; Häring, M.; Díaz Díaz, D.; Saldias, C. Effects of the Solvent Vapor Exposure on the Optical Properties and Photocatalytic Behavior of Cellulose Acetate/Perylene Free-Standing Films. *Polymers* **2023**, *15*, 2787. <https://doi.org/10.3390/polym15132787>

Academic Editor: Wei Guo

Received: 19 May 2023

Revised: 20 June 2023

Accepted: 21 June 2023

Published: 23 June 2023



Copyright: © 2023 by the authors. Licensee MDPI, Basel, Switzerland. This article is an open access article distributed under the terms and conditions of the Creative Commons Attribution (CC BY) license (<https://creativecommons.org/licenses/by/4.0/>).

1. Introduction

During the last two decades, organic molecules that are photoactive under visible light have been intensively studied due to their wide range of potential applications of current technological importance, such as light-emitting devices [1], sensors [2], solar cells [3], energy conversion [4], and photocatalysis [5] to name a few. In this sense, to exploit the photofunctionality of this type of molecules, some of the strategies followed are mainly based on chemical modification or blends with other organic agents having compatible or complementary optical properties [6,7]. These strategies have important implications for the absorption and emission light behaviors of the photoactive materials [8,9]. Considering these strategies, perylenes (Pr) intended for use as photoactive materials have shown considerable absorption response in the visible zone of the light spectrum [10,11]. For example, based on both their physical (solubility, optical absorption) and chemical (structure, functionality) molecular properties [12–14], numerous perylene derivatives have been extensively studied as dyes and paints in various industrial fields. In general, these systems

exhibit an appreciable thermal and chemical stability which allows the coating or functionalization of surfaces as an example [15,16]. Additionally, at present, Pr systems stand out for their photophysical properties, such as high quantum yields, photochemical stability, and a marked electron acceptor character [17,18]. Considering the above factors, various perylene derivatives have been used in various electronic and optical applications, such as organic photovoltaic cells [19], photoelectrodes [20], and artificial photosynthesis [21]. Despite their highly desirable optical and electronic attributes, one of the main drawbacks of Pr systems (in addition to other photoactive organic molecules) is that they do not by themselves form handleable flexible films that could potentially be integrated into photosensitive multilayer circuits or arrays [22,23]. Consequently, this issue considerably limits the possibility of expanding the range of technologically important Pr applications [24]. Accordingly, when using Pr, it is desirable to achieve an appropriate chemical stability over time and ensure a continuous interfacial contact area and homogeneous distribution in the presence of other photoactive layers in addition to increasing photostability to prolong its useful life. Therefore, the incorporation of photoactive molecules into transparent polymer films could be a plausible strategy to achieve a suitable balance between the stability of photophysical properties and their cost-effective performance in a specific application [25,26]. According to this approach, various polymeric materials displaying film-forming capabilities can be obtained from different biomass resources [27,28]. In this context, cellulose derivatives emerge as ideal candidates because they are readily available, abundant, renewable, low-cost, and inert matrices that can host various types of molecules. Particularly, cellulose acetate (CA) is one of the most important cellulose esters and shows the capability to form transparent thin films under mild experimental conditions obtained from the acetylation of cellulose, a characteristic that favorably influences its solubility and processability properties [29,30]. In addition, CA in a film format turns out to be free-standing and transparent, and possesses good thermal, mechanical, and optical properties [31]. Therefore, it can be foreseen that the combination of the attributes of polymeric materials derived from biomass and the photophysical and photocatalytic properties of perylene derivatives would allow “all-organic” photofunctional materials to be obtained.

In addition, in the literature, it has been reported that the surface morphology of films of different nature and thickness can be altered in some way by exposure to a determined solvent vapor [32–34]. In this way, this type of treatment has direct effects on the topographic and optical properties of the material [35]. Several authors attribute this behavior to the preferential orientation of regions or functional groups towards the environment saturated with solvent vapor [32,34,36,37]. Thereby, these types of strategies could be used to explore the above-mentioned effects on photoactive materials and their performance in specific chemical environments.

On the other hand, numerous investigations have used high power irradiation sources (300–1000 W) to study photocatalytic processes [38–40]. In addition, to the best of our knowledge, the use of low power light (such as light-emitting diodes [LEDs]) in photocatalysis using polymeric films was further investigated recently [37]. The latter results in a very promising approach to use low energy sources to trigger photodegradation processes mediated by photoactive polymeric films. Therefore, the use of LED radiation sources for photocatalytic processes involving independent photoactive polymeric films is of highly scientific and technological interest. Thus, a viable and innovative strategy can be developed to utilize “all-organic” biobased, free-standing, optically transparent, and photofunctional polymeric materials for applications in the field of photocatalysis. In this work, we focused our attention on the preparation, characterization, and study of the optical and photocatalytic properties of optically transparent and free-standing CA/Pr films influenced by exposure to DMF vapor. Specifically, the properties specific for the catalytic photodegradation reaction of methylene blue were investigated under cold-white LED irradiation. Characterization of the resulting films was carried out using ultraviolet/visible (UV/vis) spectroscopy, contact angle, and atomic force microscopy (AFM) techniques. In addition, theoretical electronic calculations were conducted to obtain better insight into

the geometric and energetic parameters in addition to the nature of the participating intermolecular interactions that determine and govern the optical and photocatalytic properties of CA/Pr systems.

2. Experimental Section

2.1. Materials

Cellulose acetate (39.7 wt.% acetyl content, \overline{M}_n ca. 50,000) was used as received from Sigma-Aldrich, Germany. Merck S.A supplied organic solvents. Perylene derivative (purity > 98%) was kindly provided by Professor Dr. David Diaz from the Universidad de La Laguna. The water used in all experiments was purified by a Millipore Milli-Q system (resistivity higher than 18.2 M Ω cm).

2.2. Preparation of CA/Pr Free-Standing Films

Film samples were prepared using the solution-casting method directly from stock solutions of perylene (Pr) and cellulose acetate (CA) in acetone [41]. The concentrations of Pr and CA in the acetone solution were 1.0% *w/v* (250 mg) and 5% *w/v* (2.5 g), respectively. To achieve different Pr concentrations in the films, the mixed solutions were adjusted to contain 0.3% *w/w* and 0.8% *w/w* of Pr. After vigorous stirring for 8 h, the solutions were poured into Petri dishes and air-oven dried at 35 °C for 24 h. The resulting CA/Pr free-standing films were labeled as CA/Pr 0.3% and CA/Pr 0.8%.

2.3. Characterization Techniques

The film samples were analyzed using an Agilent Cary 60 spectrophotometer to record their UV/vis spectra. Water contact angles were measured using an optical contact angle apparatus (Data physics OCA20 system) equipped with a high-resolution CCD camera and SCA 20 software (Data Physics Instruments). The initial water contact angle (θ_0) was determined by triplicate measurements, depositing a droplet of 10.0 ± 0.2 μ L on the film surface. Both the support and injecting syringe were kept at a temperature of 25.0 °C. The surface films were characterized using a 3110-Nanoscope IV atomic force microscope (AFM) in tapping mode. Film thicknesses were measured in ten random points in each sample using a handheld digimatic micrometer (Mitutoyo Corp., Kawasaki, Japan), resulting in an approximate thickness of 25.0 μ m.

2.4. Solvent Vapor Exposure Experiments

For these experiments, CA/Pr films were exposed at different times to saturated DMF solvent vapors in a closed container maintained at 40 °C for 6 h. After exposure to DMF vapors, the films were then placed in a vacuum oven at 30 °C for 24 h to study their optical, wettability, and topographical properties at certain time intervals.

The optical bandgap (E_g) was estimated from equation [42]:

$$E_g = \frac{1240}{\lambda_{th}} \quad (1)$$

in which E_g represents the optical energy bandgap (in eV), and λ_{th} is the threshold wavelength (in nm) at the onset of the absorption spectrum. The above mathematical expression is recognized as valid for conjugated aromatic organic systems, such as Pr.

The kinetic resulting data were processed considering a pseudo-first order mechanism with respect to the absorbance of each of the films. Consequently, the mathematical expression shown below was [43]:

$$\ln A_{tCA/Pr} = \ln A_{0CA/Pr} - k'_{CA/Pr} t \quad (2)$$

in which $k'_{CA/Pr}$ is the apparent rate constant and $A_{tCA/Pr}$ y $A_{0CA/Pr}$ are the absorbance values at time t and initial time, respectively. Therefore, a plot of $\ln A_{tCA/Pr}$ vs t yields $k'_{CA/Pr}$ as slope.

2.5. Photocatalysis Experiments

The study of photocatalytic performance of the as-prepared CS/Pr polymer films was carried out under visible-light irradiation using a cold-white ($\lambda_{\max} = 447$ nm and $\lambda_{\max} = 560$ nm) LED illumination source (LumiledsTM, 3 W/m²) and 20 pieces of surface mounted diodes. Specifically, the evaluation of the photocatalytic activities of the CA/Pr films was performed by immersion of the respective samples (2 cm × 2 cm) into 10 mL of a 1.5 mM methylene blue (MB) aqueous solution. Once the system was prepared, it was left in the dark for 2 h until the equilibrium state between room temperature and controlled stirring was reached. Changes in the absorbance of the dye were monitored using UV/vis spectroscopy at 650 nm (the wavelength of the maximum absorption of MB).

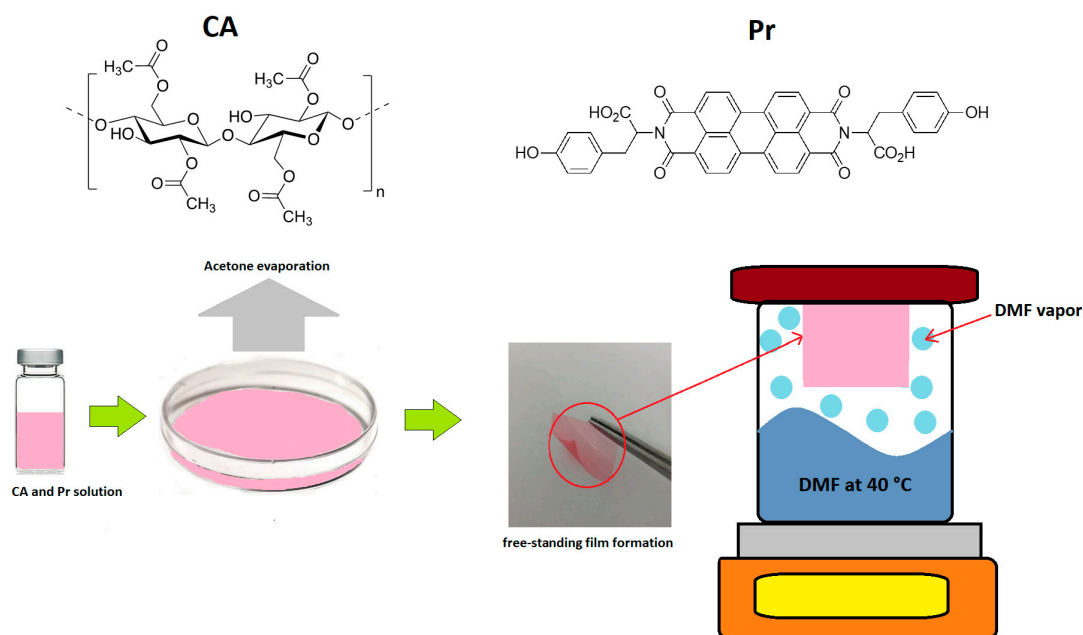
To investigate the eventual influence of non-exposed and exposed films on the kinetics of this reaction, an expression similar to Equation (2) was employed [44]:

$$\ln A_{tMB} = \ln A_{0MB} - k'_{MB} t \quad (3)$$

where A_{tMB} y A_{0MB} represent the absorbance values of MB that correspond to time t and the initial time, respectively. k'_{MB} is the apparent rate constant for photodegradation of MB.

3. Results and Discussion

Details on the experimental route used for the synthesis of the Pr can be found elsewhere [45]. Conveniently, the chemical structures of CA and Pr and the film fabrication strategy in addition to the DMF exposure process are shown in Scheme 1. It is important to mention that low Pr contents were used so as not to drastically affect the handleability of the formed CA/Pr films, an effect that currently represents a drawback with this type of polymer systems [46].



Scheme 1. Chemical structure of cellulose acetate and perylene (CA and Pr, respectively). Illustrative representation of the fabrication of CA/Pr films and the dimethylformamide (DMF) exposure process.

3.1. Optical Properties

Initially, the behavior of CA/Pr films exposed to DMF vapors was studied in terms of their optical, wettability, and topographical properties. Specifically, a systematic monitoring of the different mentioned properties depending on the exposure time was conducted (Figure 1). Monitoring of the optical behavior revealed notable increases in the respective absorbance values for the samples exposed to the solvent. Initially, the spectra of the 0.3%

and 0.8% CA/Pr films showed two absorption maxima at approximately 500 and 560 nm in addition to a shoulder at approximately 460 nm. These bands would be consistent with the characteristics of transition energies of the type $S_0 \rightarrow S_1$ (e.g., 0–0, 0–1, and 0–2). Interestingly, in both cases, the absorbance of the film samples exposed to DMF vapors increased markedly over the measured time interval. In the case of the 0.3% sample, it could be observed that as the exposure time to DMF vapor increased, a slight shift toward blue occurred, which could be attributed to the change in the environment of the Pr entities. Presumably, the vicinities of each of these molecules are gradually enriched with larger domains of aromatic rings and electron donor–acceptor functional groups. This process could be attributed to the change in the ratio of the absorbances of the bands at 560 and 500 nm that strongly depend on the spatial distance between these molecules. For the CA/Pr 0.8% sample, very slight redshifts were detected since increasing the concentration of Pr molecules in the polymer matrix favors an environment that is abundant in electrons from aromatic systems. The gradual increase in absorbance by virtue of exposure time to DMF vapor suggests that the probability of electronic transitions increases due to changes in the micropolarity, microviscosity, and dielectric attributes of the surrounding chemical environment of the Pr molecules. In this sense, the functional groups of the CA polymer could also contribute to this behavior by orienting toward the DMF vapor-saturated medium after a certain time interval.

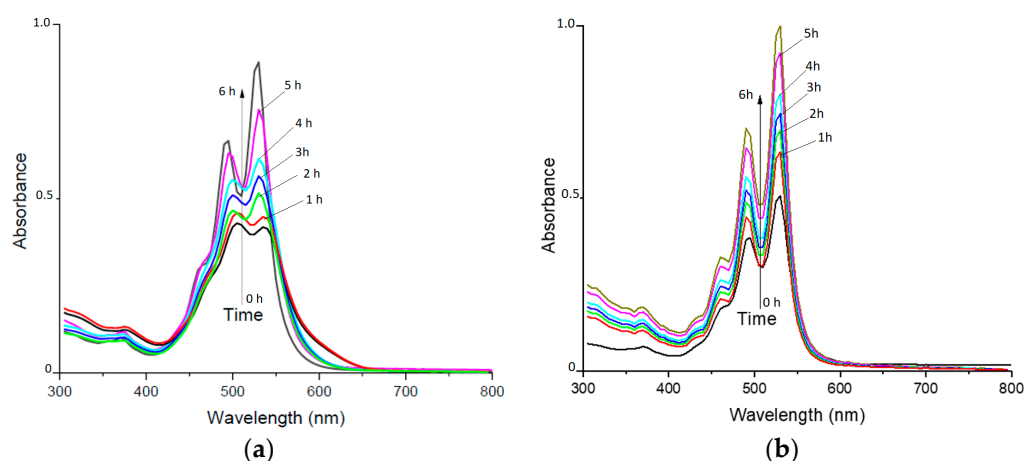


Figure 1. Ultraviolet/visible (Uv/vis) spectra of (a) cellulose acetate/perylene (CA/Pr) 0.3% and (b) CA/Pr 0.8% films exposed to dimethylformamide (DMF) vapor for 6 h.

The E_g values (Equation (1)) for the CA/Pr 0.3% and 0.8% films were 2.0 and 2.2 eV, respectively. As expected, the presence, chemical structure, and concentration of Pr in the CA matrix contribute to the processes of charge mobility and electron transfer in the solid phase, which helps explain the values of the optical bandgap values for each of the samples.

Complementarily, kinetic studies based on absorbance changes over time due to exposure to DMF vapors were conducted (Figure 2). The values of $k'_{CA/Pr}$ (Equation (2)) for CA/Pr 0.3% y CA/Pr 0.8% are $1.78 \cdot 10^{-3} \pm 7.1 \cdot 10^{-4} \text{ s}^{-1}$ y $2.07 \cdot 10^{-3} \pm 5.4 \cdot 10^{-4} \text{ s}^{-1}$, respectively. Apparently, the fit of the kinetic data along with the estimated values of rate constants would corroborate that the process of change in the optical properties of the films would be the responsibility mainly of a single species, in this case Pr. This finding agreed with the absorbance changes observed mainly in the visible region of the spectra.

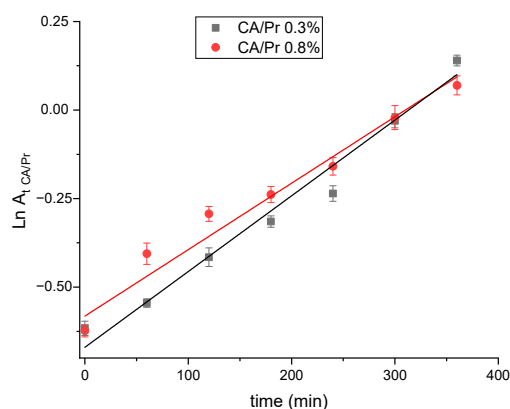


Figure 2. Rates of increase in absorbances of CA/Pr 0.3% (black line) and CA/Pr 0.8% (red line) films exposed to DMF vapor after fitting to a pseudo-first order model.

3.2. Wettability Properties

Contact angle measurements using water were conducted to study the changes in the surface properties of the CA/Pr films in terms of the hydrophilic/hydrophobic balance that were induced by the exposure time to DMF vapors. Figure 3 shows the profiles and contact angle values (θ) for CA/Pr as a function of exposure time. In both cases, a gradual increase in the values of θ over time could be observed. This phenomenon could be explained because the spreading of the drop on the surface of the film prevails in the initial stage (at $t = 0$, prior to exposure to DMF vapor) since these regions would be enriched in more hydrophilic groups originating from the matrix of CA. Note that the value of this angle is larger for the CA/Pr 0.8% sample, which could be attributed to the higher concentration of Pr in the polymeric matrix, which gives this material a more marked hydrophobic character. Additionally, as the exposure time progresses, the phenomenon of adsorption of water drops on the film's surface becomes predominant. It is likely that the response exhibited by the perylene molecules present in the polymer matrix is mediated by their selective interaction with DMF, which promotes a change in the surface morphology of the films. This change could be triggered by preferential orientation of the chemical skeleton or functional groups of the Pr toward the polymer–solvent vapor interface during the exposure period.

	Time (h)						
	0	1	2	3	4	5	6
CA/Pr 0.3%	48.1°±0.2	51.8°±0.6	54.7°±0.8	56.1°±0.1	59.2°±0.1	59.9°±0.3	61.3°±0.1
CA/Pr 0.8%	56.2°±0.3	59.5°±0.4	60.7°±0.1	62.4°±0.1	64.8°±0.4	66.0°±0.3	66.7°±0.2

Figure 3. Contact angle profiles and values ($N = 3$) for the samples for the samples CA/Pr 0.3% and CA/Pr 0.8% at different times of exposure to DMF vapors.

3.3. Topographical Properties

AFM images at different times of exposure to DMF vapors of CA/Pr films are shown in Figure 4. For both samples prior to exposure, a relatively smoother surface and relatively homogeneous topography could be observed. After 3 h of exposure, the topography undergoes a noticeable change, which was mainly demonstrated by the increase in surface roughness. At the end of the exposure time, the surface roughness increased significantly, thus accounting for the formation of microaggregates or microphases. These detected

variations were consistent with the root mean square (RMS) roughness values of each of the samples at different exposure times (Table 1). Specifically, the RMS values tended to increase for both systems as the exposure time progressed. These observations are consistent with the mentioned above phenomena since they would account for the selectivity of the DMF vapor toward the Pr entities susceptible to being promoted to rearrangements and reorganization at the micro-nanoscale level in the polymeric matrix surface. Note that the Pr concentration also plays a role in the surface morphology. This finding was confirmed since the CA/Pr 0.3% and CA/Pr 0.8% films show a morphology of the microaggregates that tend to be more rounded and sharper, respectively, after 6 h of exposure. In this sense, the 0.8% concentration sample confirms a larger amount of Pr entities that are organized toward the DMF polymer–vapor interface, conditioning the appearance of smoother or accentuated shapes that are determinant in the roughness of the surface.

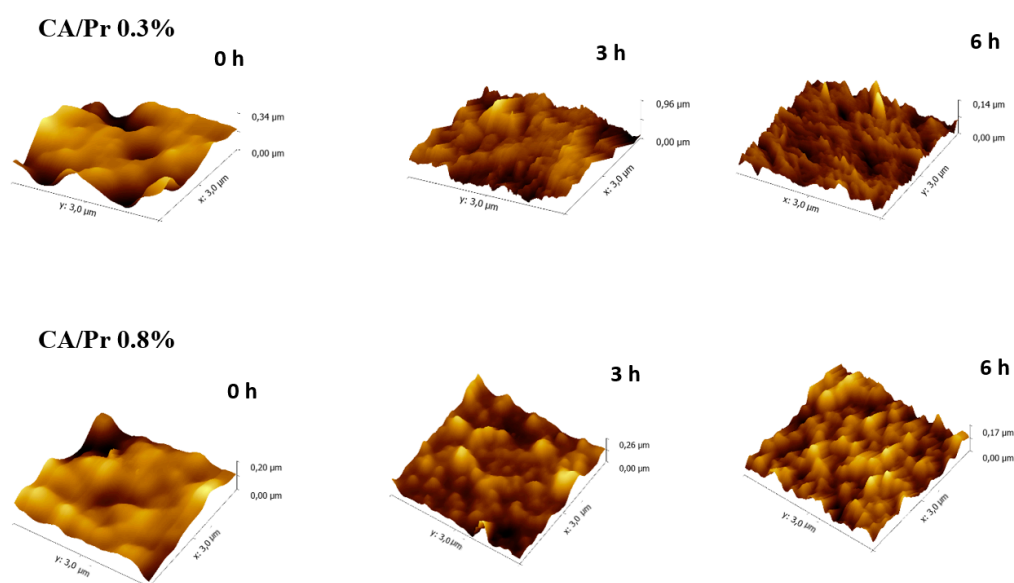


Figure 4. ($3 \times 3 \mu\text{m}^2$) Atomic force microscopy (AFM) images of CA/Pr 0.3% and CA/Pr 0.8% at different times of exposure to DMF solvent vapor.

Table 1. Root-mean-square roughness (RMS) values determined by AFM for CA/Pr 0.3% and CA/Pr 0.8% films, at different times of DMF vapor exposure.

Film	RMS (nm)		
	0 h	3 h	6 h
CA/Pr 0.3%	0.8	1.7	2.5
CA/Pr 0.8%	1.1	1.4	2.0

3.4. Photocatalysis Studies

To examine the photocatalytic properties of the prepared films, the degradation of MB was monitored as a model reaction in the presence of the CA/Pr 0.8% sample before and after exposure to solvent vapor. This reaction was selected because numerous reports in the literature are available in which different perylene derivatives act as photomediators for the degradation of methylene blue using light radiation. Figure 5 displays the monitoring of the photodegradation process using a white LED light of MB mediated by the presence of the CA/Pr film before and after exposure to DMF vapors. In both cases, the decrease in the band centered at 650 nm could be clearly noticed over time (for a total of 7 h of monitoring).

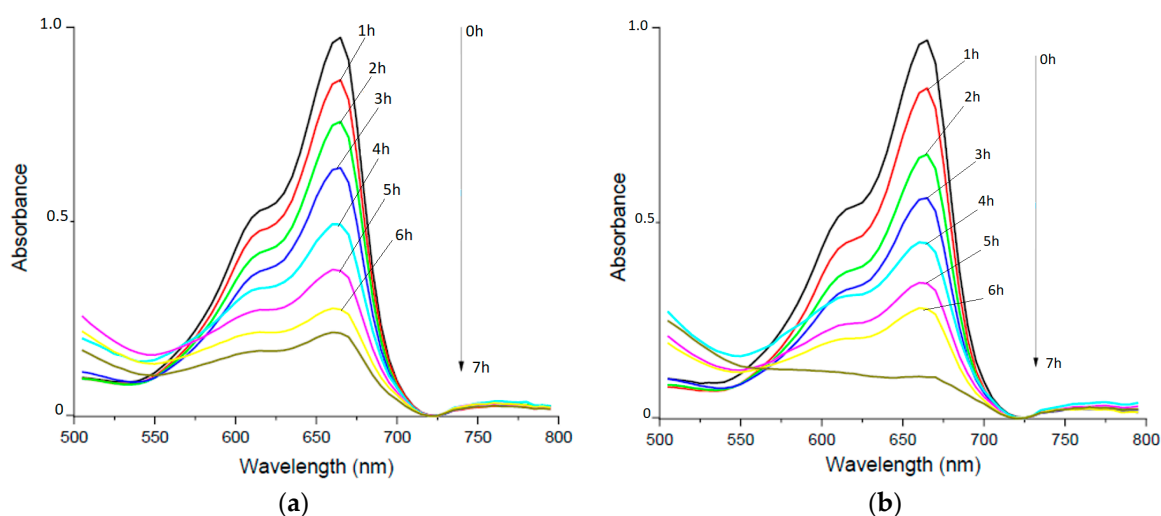


Figure 5. Spectrophotometric monitoring of methylene blue (MB) photodegradation, mediated by CA/Pr 0.8% films (a) not exposed and (b) exposed to DMF vapor. Note that white LED light was used to carry out these processes.

Figure 6 shows the plots of $\ln A_{tMB}$ vs t from which k'_{MB} can be estimated considering the slopes (Equation (3)) in both cases (namely, films exposed and not exposed to DMF vapor). Accordingly, the values of k'_{MB} for non-exposed and exposed CA/Pr were $0.13 \pm 0.010 \text{ s}^{-1}$ and $0.27 \pm 0.019 \text{ s}^{-1}$, respectively. Interestingly, the value of the constant is approximately two times for the exposed film with respect to the non-exposed film. It is likely that the change in the optical properties (such as the increase in absorbance) of the film after exposure to DMF vapor influences the photocatalytic performance in MB degradation. Apparently, these acquired attributes for the exposed system would help improve light-mediated processes. Although no pronounced shifts in the absorbance wavelength for each of the experiments were detected, the increases in absorbance for the exposed films can be related to a certain increase in the electronic transition probability, such as in the $n-\pi^*$ types. Eventually, this type of transition would be the main contributor to its behavior for the most efficient absorption of light. Note that the same reaction was tested in the absence of the CA/Pr systems under white light irradiation. Additionally, the reaction was performed in the presence of the CA/Pr systems under dark conditions. In both experiments, it was confirmed that the reaction does not proceed under the conditions described above since no significant changes were detected at 650 nm for MB in the UV/vis absorption spectrum. Consequently, the changes that were detected in the surface properties of the films after their exposure to DMF vapor could play an important role in the catalytic photodegradation process of MB. As an example, it was observed that the roughness of the films increased significantly after treatment with DMF vapor. The variation in this parameter was reflected by the increase in the number of active sites at which the MB adsorption–desorption phenomena occur onto the surface of the CA/Pr film. Thus, alterations in both the initial optical and surface properties upon the solvent vapor treatment would result in advantageous cooperative phenomena for the photocatalytic degradation process of MB.

On the other hand, the photoactivity and reuse of CA/Pr 0.8% films exposed or not exposed to DMF vapor were preliminarily evaluated during four consecutive cycles of MB photodegradation reaction. For this evaluation, the films were washed and rinsed with Milli-Q water after each use cycle. The photocatalytic activity (PA) of the films was estimated using Equation (4) [45]:

$$PA\% = \frac{k_x}{k_1} \times 100; x = 1, 2, 3 \text{ and } 4 \quad (4)$$

in which k_x and k_1 correspond to the MB photodegradation rate of each of the cycles after use and the photodegradation rate of the 1st cycle, respectively.

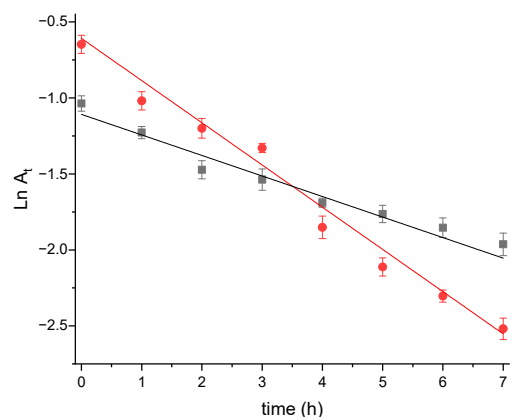


Figure 6. MB photodegradation rates mediated by CA/Pr 0.8% films unexposed (black line) and exposed (red line) to DMF vapor.

Importantly, Figure 7 shows that the reusability and photoactivity of the non-exposed films and DMF vapor-exposed films in the MB photodegradation process did not experience a severe decrease in their respective performances after each cycle. This process is a very relevant aspect since the untreated and DMF-treated free-standing “all-organic” films showed a relatively constant performance for the number of cycles to which they were subjected. This process would help confirm that the DMF vapor treatment of CA/Pr 0.8% films does not drastically affect their reusability in the photodegradation of MB in aqueous medium. Presumably, the mechanism that prevails in the photodegradation process would consist of three consecutive stages: (1) adsorption of MB on the surface of the film, (2) photodegradation induced by light (such as appearance and intervention of reactive oxygen species [ROS]), and (3) desorption of the species that result as products of photodegradation. According to these antecedents, the presence of Pr along with DMF vapor treatment of CA/Pr films provides a viable strategy for improving the efficiency and activity of the MB photodegradation catalytic process. It is important to highlight that these types of systems offer explorable alternatives for scaling-up due to their versatility, potentially low toxicity for use in bodies of water, low-cost fabrication, high availability of components, and easy processability for light-induced chemical reactions of technological importance. In this way, these types of photoactive materials would be emerging alternatives for photodegradation of a wide variety of organic dyes in bodies or aqueous media.

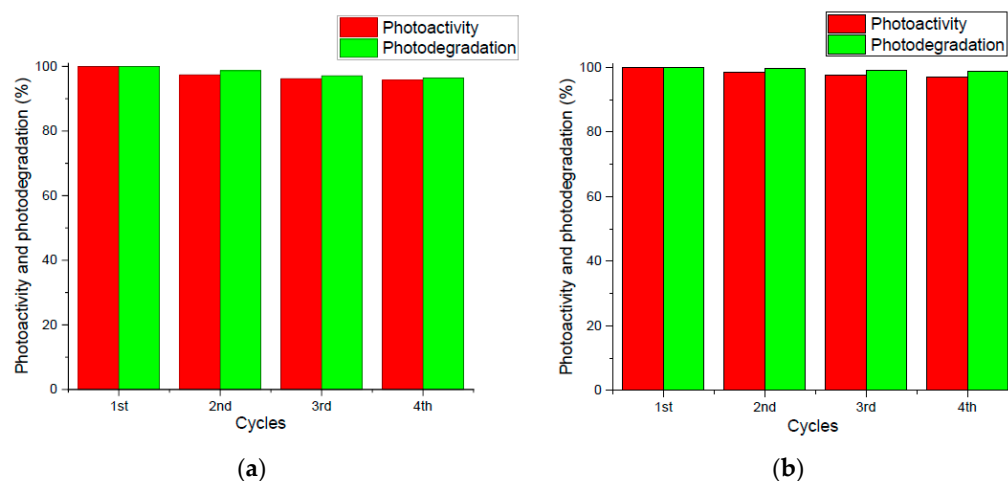


Figure 7. The photodegradation of MB and the photoactivity of CA/Pr 0.8% films (a) not exposed and (b) exposed to DMF vapor upon each cycle of use.

4. Conclusions

The presented route is a relatively simple method for the fabrication of free-standing “all-organic” CA/Pr photoactive films containing low amounts of a Pr. Consequently, the optical, wettability, and topographical properties of these films were convincingly modified by exposure to DMF vapors. The change in these properties were found to influence the photocatalytic performance of the films against MB dye degradation using a white LED light. Interestingly, the systems exposed to DMF vapors reached a higher MB photodegradation rate value compared with those that were not exposed. Additionally, the photoactivity and reusability of both non-exposed and exposed films in the photodegradation of MB were not drastically affected during each of the four cycles to which they were subjected. Finally, this study exposes a scalable and comparatively economically viable strategy (organic materials only) for potential applications in photodegradation of organic dyes in water bodies.

Author Contributions: G.C. and M.H.: Investigation, Experimental analysis; A.C.: Data curation, Validation, Visualization; O.R. and S.B.: Conceptualization, Formal analysis; A.L. and D.D.D.: Supervision, Writing—original draft; C.S.: Funding acquisition, Writing—review and editing. All authors have read and agreed to the published version of the manuscript.

Funding: This research was funded by the FONDECYT project 1211022.

Institutional Review Board Statement: Not applicable.

Informed Consent Statement: Not applicable.

Data Availability Statement: The data presented in this study are available upon request from the corresponding author.

Acknowledgments: The authors thank FONDECYT projects 1211022 (C.S.). D.D.D. also thanks the Spanish Ministry of Science and Innovation for the Senior Beatriz Galindo Award (BEAGAL18/00166) and NANOTec, INTech, Cabildo de Tenerife, and ULL for laboratory facilities. S.B. thanks MINECO for a Juan de la Cierva-Formacion contract (FJC2019-039515-I). D.D.D. thanks NANOTec, INTech, Cabildo de Tenerife and ULL for laboratory facilities.

Conflicts of Interest: The authors declare no conflict of interest.

References

1. Cicoira, F.; Santato, C. Organic Light Emitting Field Effect Transistors: Advances and Perspectives. *Adv. Funct. Mater.* **2007**, *17*, 3421–3434. [[CrossRef](#)]
2. Lee, Y.H.; Kweon, O.Y.; Kim, H.; Yoo, J.H.; Han, S.G.; Oh, J.H. Recent Advances in Organic Sensors for Health Self-Monitoring Systems. *J. Mater. Chem. C Mater.* **2018**, *6*, 8569–8612. [[CrossRef](#)]
3. Duan, L.; Uddin, A. Progress in Stability of Organic Solar Cells. *Adv. Sci.* **2020**, *7*, 1903259. [[CrossRef](#)] [[PubMed](#)]
4. Sharma, A.; Masoumi, S.; Gedefaw, D.; O’Shaughnessy, S.; Baran, D.; Pakdel, A. Flexible Solar and Thermal Energy Conversion Devices: Organic Photovoltaics (OPVs), Organic Thermoelectric Generators (OTEGs) and Hybrid PV-TEG Systems. *Appl. Mater. Today* **2022**, *29*, 101614. [[CrossRef](#)]
5. Rahman, M.; Tian, H.; Edvinsson, T. Revisiting the Limiting Factors for Overall Water-Splitting on Organic Photocatalysts. *Angew. Chem.* **2020**, *132*, 16418–16433. [[CrossRef](#)]
6. Shao, Q.; Xing, B. Photoactive Molecules for Applications in Molecular Imaging and Cell Biology. *Chem. Soc. Rev.* **2010**, *39*, 2835. [[CrossRef](#)]
7. Mola, G.T.; Dlamini, W.E.; Oseni, S.O. Improving Optical Absorption Bandwidth Using Bi-Layer Bulkheterojunction Organic Photoactive Medium. *J. Mater. Sci. Mater. Electron.* **2016**, *27*, 11628–11633. [[CrossRef](#)]
8. Yan, D.; Lu, J.; Wei, M.; Qin, S.; Chen, L.; Zhang, S.; Evans, D.G.; Duan, X. Heterogeneous Transparent Ultrathin Films with Tunable-Color Luminescence Based on the Assembly of Photoactive Organic Molecules and Layered Double Hydroxides. *Adv. Funct. Mater.* **2011**, *21*, 2497–2505. [[CrossRef](#)]
9. Bianco, A.; Minella, M.; De Laurentiis, E.; Maurino, V.; Minero, C.; Vione, D. Photochemical Generation of Photoactive Compounds with Fulvic-like and Humic-like Fluorescence in Aqueous Solution. *Chemosphere* **2014**, *111*, 529–536. [[CrossRef](#)]
10. Cai, S.; Shi, H.; Li, J.; Gu, L.; Ni, Y.; Cheng, Z.; Wang, S.; Xiong, W.; Li, L.; An, Z.; et al. Visible-Light-Excited Ultralong Organic Phosphorescence by Manipulating Intermolecular Interactions. *Adv. Mater.* **2017**, *29*, 1701244. [[CrossRef](#)]
11. Mo, Z.; Di, J.; Yan, P.; Lv, C.; Zhu, X.; Liu, D.; Song, Y.; Liu, C.; Yu, Q.; Li, H.; et al. An All-Organic D-A System for Visible-Light-Driven Overall Water Splitting. *Small* **2020**, *16*, 2003914. [[CrossRef](#)] [[PubMed](#)]

12. Chen, S.; Slattum, P.; Wang, C.; Zang, L. Self-Assembly of Perylene Imide Molecules into 1D Nanostructures: Methods, Morphologies, and Applications. *Chem. Rev.* **2015**, *115*, 11967–11998. [[CrossRef](#)] [[PubMed](#)]
13. Avlasevich, Y.; Li, C.; Müllen, K. Synthesis and Applications of Core-Enlarged Perylene Dyes. *J. Mater. Chem.* **2010**, *20*, 3814. [[CrossRef](#)]
14. Gupta, R.K.; Sudhakar, A.A. Perylene-Based Liquid Crystals as Materials for Organic Electronics Applications. *Langmuir* **2019**, *35*, 2455–2479. [[CrossRef](#)]
15. Krieg, E.; Niazov-Elkan, A.; Cohen, E.; Tsarfati, Y.; Rybtchinski, B. Noncovalent Aqua Materials Based on Perylene Diimides. *Acc. Chem. Res.* **2019**, *52*, 2634–2646. [[CrossRef](#)]
16. Rahmati, M.; Dayneko, S.V.; Pahlevani, M.; Welch, G.C. Interlayer Engineering of Flexible and Large-Area Red Organic-Light-Emitting Diodes Based on an N-Annulated Perylene Diimide Dimer. *ACS Appl. Electron. Mater.* **2020**, *2*, 48–55. [[CrossRef](#)]
17. Fennel, F.; Gershberg, J.; Stolte, M.; Würthner, F. Fluorescence Quantum Yields of Dye Aggregates: A Showcase Example Based on Self-Assembled Perylene Bisimide Dimers. *Phys. Chem. Chem. Phys.* **2018**, *20*, 7612–7620. [[CrossRef](#)]
18. Shivanna, R.; Shoaee, S.; Dimitrov, S.; Kandappa, S.K.; Rajaram, S.; Durrant, J.R.; Narayan, K.S. Charge Generation and Transport in Efficient Organic Bulk Heterojunction Solar Cells with a Perylene Acceptor. *Energy Environ. Sci.* **2014**, *7*, 435–441. [[CrossRef](#)]
19. Kozma, E.; Catellani, M. Perylene Diimides Based Materials for Organic Solar Cells. *Dye. Pigment.* **2013**, *98*, 160–179. [[CrossRef](#)]
20. Shan, B.; Nayak, A.; Brennaman, M.K.; Liu, M.; Marquard, S.L.; Eberhart, M.S.; Meyer, T.J. Controlling Vertical and Lateral Electron Migration Using a Bifunctional Chromophore Assembly in Dye-Sensitized Photoelectrosynthesis Cells. *J. Am. Chem. Soc.* **2018**, *140*, 6493–6500. [[CrossRef](#)]
21. Ryan, S.T.J.; Young, R.M.; Henkelis, J.J.; Hafezi, N.; Vermeulen, N.A.; Hennig, A.; Dale, E.J.; Wu, Y.; Krzyaniak, M.D.; Fox, A.; et al. Energy and Electron Transfer Dynamics within a Series of Perylene Diimide/Cyclophane Systems. *J. Am. Chem. Soc.* **2015**, *137*, 15299–15307. [[CrossRef](#)] [[PubMed](#)]
22. Adams, V.; Cameron, J.; Wallace, M.; Draper, E.R. Mechanoresponsive Self-Assembled Perylene Bisimide Films. *Chem. —A Eur. J.* **2020**, *26*, 9879–9882. [[CrossRef](#)]
23. Damaceanu, M.-D.; Rusu, R.-D.; Bruma, M. Copolyimides Containing Perylene and Hexafluoroisopropylidene Moieties. *High Perform. Polym.* **2012**, *24*, 50–57. [[CrossRef](#)]
24. Zhang, F.; Ma, Y.; Chi, Y.; Yu, H.; Li, Y.; Jiang, T.; Wei, X.; Shi, J. Self-Assembly, Optical and Electrical Properties of Perylene Diimide Dyes Bearing Unsymmetrical Substituents at Bay Position. *Sci. Rep.* **2018**, *8*, 8208. [[CrossRef](#)]
25. Kim, W.S.; Yoon, H.I.; Lee, J.M.; Hwang, T.G.; Kim, H.M.; Lee, H.K.; Kim, S.; Choi, W.J.; Kim, J.P. Substituents Effects on Properties of Perylene Dyes for Spectrum Conversion Film. *Dye. Pigment.* **2023**, *209*, 110845. [[CrossRef](#)]
26. El-Bashir, S.M.; Al-Jaghawani, A.A. Perylene-Doped Polycarbonate Coatings for Acrylic Active Greenhouse Luminescent Solar Concentrator Dryers. *Results Phys.* **2020**, *16*, 102920. [[CrossRef](#)]
27. Wang, J.; Xun, Z.; Zhao, C.; Liu, Y.; Gu, J.; Huo, P. Converting Soy Protein Isolate into Biomass-Based Polymer Electrolyte by Grafting Modification for High-Performance Supercapacitors. *Int. J. Biol. Macromol.* **2022**, *209*, 268–278. [[CrossRef](#)]
28. Tao, Y.; Zhou, J.; Wang, J.; Wang, Y.; Sun, J.; Fang, Q. High Performance Low Dielectric Constant Polymer with Good Film-Forming Ability Developed from Renewable Plant Oil (Anethole). *Macromol. Chem. Phys.* **2018**, *219*, 1800133. [[CrossRef](#)]
29. Monisha, S.; Mathavan, T.; Selvasekarapandian, S.; Benial, A.M.F.; Latha, M.P. Preparation and Characterization of Cellulose Acetate and Lithium Nitrate for Advanced Electrochemical Devices. *Ionics* **2017**, *23*, 2697–2706. [[CrossRef](#)]
30. Xu, S.; Zhou, H.; Jia, H.; Xu, J.; Ma, L.; Zang, Y.; Jiang, P.; Ma, W.; Zhang, Y.; Zhao, W.; et al. Preparation and High Performance of Cellulose Acetate Films by Grafting with Imidazole Ionic Liquid. *ACS Omega* **2021**, *6*, 12500–12506. [[CrossRef](#)]
31. Rajeswari, A.; Christy, E.J.S.; Swathi, E.; Pius, A. Fabrication of Improved Cellulose Acetate-Based Biodegradable Films for Food Packaging Applications. *Environ. Chem. Ecotoxicol.* **2020**, *2*, 107–114. [[CrossRef](#)]
32. Dąbczyński, P.; Wójtowicz, G.; Rysz, J. Mutual Diffusion of Model Acceptor/Donor Bilayers under Solvent Vapor Annealing as a Novel Route for Organic Solar Cell Fabrication. *Energies* **2022**, *15*, 1033. [[CrossRef](#)]
33. Sinturel, C.; Vayer, M.; Morris, M.; Hillmyer, M.A. Solvent Vapor Annealing of Block Polymer Thin Films. *Macromolecules* **2013**, *46*, 5399–5415. [[CrossRef](#)]
34. Guan, T.; Yuket, S.; Cong, H.; Carton, D.W.; Zhang, N. Permanent Hydrophobic Surface Treatment Combined with Solvent Vapor-Assisted Thermal Bonding for Mass Production of Cyclic Olefin Copolymer Microfluidic Chips. *ACS Omega* **2022**, *7*, 20104–20117. [[CrossRef](#)] [[PubMed](#)]
35. Khasim, S.; Pasha, A.; Lakshmi, M.; Chellasamy, P.; Kadarkarai, M.; Darwish, A.A.A.; Hamdalla, T.A.; Al-Ghamdi, S.A.; Alfadhli, S. Post Treated PEDOT-PSS Films with Excellent Conductivity and Optical Properties as Multifunctional Flexible Electrodes for Possible Optoelectronic and Energy Storage Applications. *Opt. Mater.* **2022**, *125*, 112109. [[CrossRef](#)]
36. Chen, W.; Zhang, X.; Tan, D.; Xu, P.; Yang, B.; Shi, K.; Zhu, B.; Liu, Q.; Lei, Y.; Liu, S.; et al. Improvement in Mechanical Properties of 3D-Printed PEEK Structure by Nonsolvent Vapor Annealing. *Macromol. Rapid Commun.* **2022**, *43*, 2100874. [[CrossRef](#)] [[PubMed](#)]
37. Sampaio, M.J.; Ribeiro, A.R.L.; Ribeiro, C.M.R.; Borges, R.A.; Pedrosa, M.F.; Silva, A.M.T.; Silva, C.G.; Faria, J.L. A Technological Approach Using a Metal-Free Immobilized Photocatalyst for the Removal of Pharmaceutical Substances from Urban Wastewaters. *Chem. Eng. J.* **2023**, *459*, 141617. [[CrossRef](#)]
38. Panthawan, A.; Sanmuangmoon, P.; Jumrus, N.; Thongpan, W.; Pooseekheaw, P.; Kumpika, T.; Sroila, W.; Kantarak, E.; Tuantranont, A.; Singjai, P.; et al. Photocatalytic Enhancement of a Novel Composite CuAl₂O₄/TiO₂/CuO Films Prepared by Sparking Process. *Optik* **2020**, *224*, 165502. [[CrossRef](#)]

39. Han, B.; Hu, Y.H. MoS₂ as a Co-catalyst for Photocatalytic Hydrogen Production from Water. *Energy Sci. Eng.* **2016**, *4*, 285–304. [[CrossRef](#)]
40. Romero, V.; De la Cruz, N.; Dantas, R.F.; Marco, P.; Giménez, J.; Esplugas, S. Photocatalytic Treatment of Metoprolol and Propranolol. *Catal Today* **2011**, *161*, 115–120. [[CrossRef](#)]
41. Mendez-López, M.; Ramos-Hernández, A.; Moreno-Serna, V.; Bonardd, S.; Ramírez, O.; Silva, H.; Inostroza-Rivera, R.; Diaz, D.D.; Leiva, A.; Saldías, C. A Facile Approach for Tuning Optical and Surface Properties of Novel Biobased Alginate/POTE Handleable Films via Solvent Vapor Exposure. *Int. J. Biol. Macromol.* **2021**, *193*, 258–268. [[CrossRef](#)] [[PubMed](#)]
42. Jessop, I.; Albornoz, J.; Ramírez, O.; Durán, B.; Molero, L.; Bonardd, S.; Kortaberria, G.; Diaz Diaz, D.; Leiva, A.; Saldías, C. Optical, Morphological and Photocatalytic Properties of Biobased Tractable Films of Chitosan/Donor-Acceptor Polymer Blends. *Carbohydr. Polym.* **2020**, *249*, 116822. [[CrossRef](#)] [[PubMed](#)]
43. Ramirez, O.; Bonardd, S.; Saldías, C.; Radic, D.; Leiva, Á. Biobased Chitosan Nanocomposite Films Containing Gold Nanoparticles: Obtainment, Characterization, and Catalytic Activity Assessment. *ACS Appl. Mater. Interfaces* **2017**, *9*, 16561–16570. [[CrossRef](#)] [[PubMed](#)]
44. Saldías, C.; Díaz, D.D.; Bonardd, S.; Soto-Marfull, C.; Cordoba, A.; Saldías, S.; Quezada, C.; Radic, D.; Leiva, Á. In Situ Preparation of Film and Hydrogel Bio-Nanocomposites of Chitosan/Fluorescein-Copper with Catalytic Activity. *Carbohydr. Polym.* **2018**, *180*, 200–208. [[CrossRef](#)] [[PubMed](#)]
45. Draper, E.R.; Walsh, J.J.; McDonald, T.O.; Zwijnenburg, M.A.; Cameron, P.J.; Cowan, A.J.; Adams, D.J. Air-Stable Photoconductive Films Formed from Perylene Bisimide Gelators. *J. Mater. Chem. C* **2014**, *2*, 5570–5575. [[CrossRef](#)]
46. Elbl, J.; Gajdziok, J.; Kolarczyk, J. 3D Printing of Multilayered Orodispersible Films with In-Process Drying. *Int. J. Pharm.* **2020**, *575*, 118883. [[CrossRef](#)]

Disclaimer/Publisher's Note: The statements, opinions and data contained in all publications are solely those of the individual author(s) and contributor(s) and not of MDPI and/or the editor(s). MDPI and/or the editor(s) disclaim responsibility for any injury to people or property resulting from any ideas, methods, instructions or products referred to in the content.